https://doi.org/10.5194/egusphere-2023-2436
Preprint. Discussion started: 11 December 2023

A change in the relationship between ENSO and the South Atlantic Subtropical Dipole in the past four decades

Lejiang Yu[1*], Shiyuan Zhong[2], Timo Vihma[3], Cuijuan Sui[4], and Bo Sun[1]

1 MNR Key Laboratory for Polar Science, Polar Research Institute of China, Shanghai, China,

2 Department of Geography, Environment and Spatial Sciences, Michigan State University, East Lansing, MI, USA,

3 Finnish Meteorological Institute, Helsinki, Finland

4 National Marine Environmental Forecasting Center, Beijing, China

*Corresponding Author's address Dr. Lejiang Yu

MNR Key Laboratory for Polar Science, Polar Research Institute of China, Shanghai, China

Jinqiao Road 451, 200136, Shanghai, China

Phone: 0086-020-58712034, email: yulejiang@sina.com.cn

https://doi.org/10.5194/egusphere-2023-2436
Preprint. Discussion started: 11 December 2023

Abstract

This study investigates the relationship between sea surface temperature (SST) in the subtropical Atlantic Ocean, as represented by the Southern Atlantic Subtropical Dipole (SASD), and SST in the tropical Pacific Ocean, identified by the El Niño-Southern Oscillation (ENSO). Our analysis reveals a significant inverse correlation between the SASD and Niño indices over a century, with multi-decadal variability that contradicts weak simultaneous correlations previously reported in the literature. The study also highlights a strengthening of their inverse correlations in the most recent two decades compared to the preceding two decades, which can be attributed to the shift in ENSO regime from more frequent eastern Pacific El Niño to central Pacific El Niño around the turn of the century. This shift helps set the stage for changes in convective activity in the critical region (20°S-40°S, 180°-140°W) of the central South Pacific Ocean, triggering wavetrains that propagate along different paths and ultimately contributing to different southern Atlantic subtropical high (SASH) and changes in anomalous SST patterns in the subtropical Atlantic Ocean. These findings advance our understanding of the interactions between South Atlantic and Pacific SST variations, which strongly influence rainfall patterns particularly in South America and southern Africa and may improve sub-seasonal to seasonal precipitation predictions in these regions.

Plain Language Summary

We look at how changes in sea surface temperature (SST) in the subtropical Atlantic

https://doi.org/10.5194/egusphere-2023-2436
Preprint. Discussion started: 11 December 2023

Ocean and the tropical Pacific Ocean are related to each other over time. We found that there is a significant inverse correlation between the two areas over the course of a century, and that this relationship changes over time in multi-decade cycles. We also found that the inverse relationship has become stronger in the recent two decades compared to the proceeding two decades. This change is likely due to a regime shift in ENSO around the turn of the century that helps set stage to the occurrences of different convective activities in a particular area of the central South Pacific Ocean, ultimately leading to changes in SST in the subtropical South Atlantic through atmospheric waves. Understanding these relationships is important because they can affect, among other things, rainfall in South America and southern Africa, and the study may help improve predictions of future rainfall patterns in these regions.

Key Points

In contrary to the current understanding, there can be a strong connection between ENSO and the South Atlantic Subtropical Dipole (SASD).

It is highly probable that the robust inverse correlation between ENSO and SASD will persist in the future.

The ENSO-SASD correlation exhibits substantial multi-decadal variability over the course of a century.

The change in the ENSO-SASD relation can be linked to changes in ENSO regime and convective activities over the central South Pacific Ocean.

https://doi.org/10.5194/egusphere-2023-2436
Preprint. Discussion started: 11 December 2023

1. Introduction

The South Atlantic subtropical dipole (SASD) mode represents an opposite variability of sea surface temperature (SST) over the northeastern and southwestern South Atlantic Ocean (Venegas et al., 1997; Sterl and Hazeleger, 2003; Haarsma et al., 2005; Morioka et al., 2011). The SASD exhibits a strong seasonal variability that peaks in austral summer and is related to the strength and location of the South Atlantic subtropical high (SASH). The anomalous surface circulations associated with SASH influence the oceanic mixed layer depth and surface evaporation, leading to SST anomalies over South Atlantic subtropical regions (Sterl and Hazeleger, 2003; Haarsma et al., 2005; Colberg and Reason, 2006; Morioka et al., 2011). Surface shortwave radiation also plays a vital role in the formation and decay of the SASD (Morioka et al., 2011).

The SASD also shows an interannual variability, which has been linked to year-to-year changes in precipitation in southern Africa (Vigaud et al., 2009; Morioka et al., 2011), West Africa (Nnamchi and Li, 2011) and South America (Muza et al., 2009; Bombaridi and Carvalho, 2011; Kayano et al., 2013; Bombardi et al., 2014). Understanding what factors are behind the SASD interannual variability may improve precipitation predictions for these regions. Previous studies have investigated the effects of large-scale climate indices on the SASD. Hermes and Reason (2005) and Morioka et al. (2014) noted the effect of the Antarctic Oscillation (AAO) on the SASD. Several studies have confirmed the linkage between the SASD and the Subtropical Indian Ocean Dipole (SIOD) (Fauchereau et al., 2003; Hermes and

https://doi.org/10.5194/egusphere-2023-2436
Preprint. Discussion started: 11 December 2023

Reason, 2005; Lin, 2019; Yu et al., 2023). A weak relationship has been noted between the simultaneous values of SASD and ENSO at zero lag (Venegas et al., 1997; Hermes and Reason, 2003; Fauchereau et al., 2003; Kayano et al., 2013). However, Kayano et al. (2013) detected a significant lagged correlation between the two indices. Rodrigues et al. (2015) explained the weak SASD-ENSO relationship by showing that although negative (positive) SASD events are associated with the positive (negative) phase of the central Pacific El Niño events, such association is absent during eastern Pacific El Niño events.

The weak simultaneous and strong lagged relationships between SASD and ENSO have been established based on data for earlier time periods prior to 2010 (Rodrigues et al., 2015). However, since 2010, there have been a major El Niño event and two record-breaking La Niña events, making the last decade invaluable for determining how robust the established SASD-ENSO relationship is. In this study, we have extended previous analyses to include the most recent decade with the aim to test the robustness of the SASD-ENSO relationship, and to offer additional insight into the mechanisms behind the teleconnection between the SST anomalies in the tropical Pacific and subtropical South Atlantic Oceans. In addition, we have expanded our analysis by examining SST time series over a course of a century dating back to 1871.

2. Datasets and methods

The monthly SST data applied in this study are from the U.S. National Oceanic and Atmospheric Administration (NOAA) Extended Reconstructed Sea Surface

https://doi.org/10.5194/egusphere-2023-2436
Preprint. Discussion started: 11 December 2023

Temperature (ERSST) version 5 (Huang et al., 2017) covering the globe with a horizontal resolution of 2.0 °latitude × 2.0 °longitude and spanning from 1871 to the present. The primary focus of our study is the recent four decades from 1979 through 2020. Following Morioka et al. (2011), we define the SASD index as the difference of the SST anomalies between the south-western (10-30° W, 30-40° S) and north-eastern (0-20° W, 15-25° S) South Atlantic Ocean (Figure 1a). The ENSO signal is represented primarily by the Niño 3.4 index, defined on the basis of SST anomalies in the tropical central Pacific Ocean (5° N-5° S, 120-170° W) (Trenberth, 1997). The relationship between ENSO and SASD is determined by the 18-year sliding correlation between the detrended time series of the SASD index and the Niño 3.4 index. Two other ENSO indices, the Niño 3 index (5° N-5° S, 90-150° W) and the Niño 4 index (5° N-5° S, 160 ° E-150 ° W), are also included in our analyses to test the sensitivity of the SASD-ENSO relationship to the types of ENSO events. The statistical significance of the correlation is determined by the two-tailed student's t test and the statistical significance of the difference between two time series of regression coefficients is tested by the Z-test (Clogg et al., 1995).

We explore the mechanisms underlying the SASD-ENSO relationship through examining the corresponding atmospheric circulations using monthly data from the European Centre for Medium-Range Weather Forecasts (ECMWF) fifth-generation reanalysis (ERA5) that has a 1/4 degree latitude and longitude horizontal resolution and covers the period from 1979 to the present (Hersbach et al., 2020). We supplement the ERA5 data with the monthly NOAA Interpolated Outgoing Longwave

https://doi.org/10.5194/egusphere-2023-2436
Preprint. Discussion started: 11 December 2023

Radiation (OLR) data, which has a horizontal resolution of 2.5° latitude × 2.5° longitude (Liebmann and Smith, 1996). To analyze atmospheric planetary waves, we calculate the 200-hPa Rossby wave source (RWS) using the formulae proposed by Sardeshmukh and Hoskins (1998):

$$\mathrm{RWS} = -V_\chi \cdot \nabla\zeta - \zeta D \approx -V_\chi' \cdot \nabla\bar{\zeta} - \bar{\zeta} D' \quad (1)$$

wherein ζ is the vertical component of the absolute vorticity, V_χ and D are the divergent wind and divergence at 200 hPa, respectively. Climatological mean and perturbation are represented by overbar and prime, respectively.

Additionally, we also analyze 200-hPa wave activity flux (WAF), which is derived using the equation proposed by Takaya and Nakamura (2001):

$$W = \frac{p\cos\phi}{2|U|}\begin{pmatrix} \frac{\bar{u}}{a^2\cos^2\phi}\left[\left(\frac{\partial\psi'}{\partial\lambda}\right)^2 - \psi'\frac{\partial^2\psi'}{\partial^2\lambda}\right] + \frac{\bar{v}}{a^2\cos\phi}\left[\frac{\partial\psi'}{\partial\lambda}\frac{\partial\psi'}{\partial\phi} - \psi'\frac{\partial^2\psi'}{\partial\lambda\partial\phi}\right] \\ \frac{\bar{v}}{a^2\cos\phi}\left[\frac{\partial\psi'}{\partial\lambda}\frac{\partial\psi'}{\partial\phi} - \psi'\frac{\partial^2\psi'}{\partial\lambda\partial\phi}\right] + \frac{\bar{v}}{a^2}\left[\left(\frac{\partial\psi'}{\partial\phi}\right)^2 - \psi'\frac{\partial^2\psi'}{\partial^2\phi}\right] \end{pmatrix}$$

(2)

Where λ and ϕ are longitude and latitude, respectively; ψ is geostrophic stream function; $|U|$ is climatological horizontal wind; $\bar{u}$ and $\bar{v}$ are the climatological zonal and meridional winds, respectively; p is the pressure divided by 1000 hPa; a is the earth's radius. Overbar symbols represent climatological values while prime symbols denote anomalies.

All the analyses presented focus on austral summer when both ENSO and SASD peak in the annual cycle. Here, austral summer refers to January, February and March (JFM) as SASD tends to peak in February (Morioka et al., 2012).

https://doi.org/10.5194/egusphere-2023-2436
Preprint. Discussion started: 11 December 2023

To further corroborate our statistical findings, we conduct numerical experiments using Version 5 of the Community Atmosphere Model (CAM5), which serves as the atmospheric component of the Community Earth System Model (CESM). CAM5 features 30 vertical levels and a horizontal resolution of 1.9 latitude × 2.5 longitude. For more in-depth information about CAM5, please refer to Neale et al. (2011).

Several numerical experiments are conducted. These experiments include a control run, which spans 50 years and is forced by the climatological annual cycle of SST and sea ice concentration data from the Hadley Center, and three idealized experiments where a +2 ℃ SST anomaly is introduced in the Southern Pacific region (20°S-40°S, 180°-140°W), the Niño4 region over the central tropical Pacific (5°N-5°S, 160°E-150°W) and the Niño3 region over the eastern tropical Pacific (5°N-5°S, 150°W-90°W), respectively. The warm SST anomaly is introduced annually from January 1 to March 31, while the SST and sea ice conditions in the remaining months and regions are maintained at climatological levels. The last 20 years of the control run are utilized as the reference years to restart the idealized experiments. The results from the numerical experiments are presented as the differences between the idealized experiments and the control experiment.

3. Results

3.1 Variability of the SASD-ENSO relationship

In contrast to the weak simultaneous correlation between the SASD and the Niño

https://doi.org/10.5194/egusphere-2023-2436
Preprint. Discussion started: 11 December 2023

3.4 indices suggested in previous studies, our results indicate a significant inverse correlation (r = -0.51, p<0.01) between the two indices (Figure 1b, c) over the period of 1979 through 2020. The magnitudes of the 18-year moving correlation coefficients of the detrended SASD index (Figure 1b) with the detrended Niño 3.4 index (Figure 1b) tripled from r ≈ -0.25 in the late-1980s to r ≈ -0.75 during 2006-2011, intercepting the p = 0.05 line between 1993 and 1994 (Figure 1c). When we divided the four decades into two equally long periods, we found that the correlation coefficient was -0.32 (p > 0.05) for the period before 2000 and -0.77 (p < 0.01) for the period after 2000. Despite replacing Niño 3.4 with Niño 4 or Niño 3 indices, the marked difference in correlation strength between the earlier and latter periods remains unchanged, which is unsurprising given the known correlation among the three Niño indices. Specifically, the correlation coefficients for Niño 4 and Niño 3 increased from -0.34 and -0.10 (p > 0.05), respectively, for the earlier period to -0.71 (p < 0.01) for both indices for the latter period. The overall correlations for the entire 42-year period were -0.4 for Niño 4 and -0.48 for Niño 3 (p < 0.05), which is slightly weaker than the correlation of -0.51 for Niño 3.4. While Kao and Yu (2009) suggested that there are superior alternatives to represent ENSO diversity than the Niño 3, 3.4 and 4 indices, the above results reveal, for the first time to our knowledge, a strong multi-decadal variability in the SASD-ENSO relationship. In other words, the interannual SST variability modes in the tropical Pacific and subtropical Atlantic Oceans are teleconnected, but the teleconnection is highly variable on the decadal to multi-decadal scale.

https://doi.org/10.5194/egusphere-2023-2436
Preprint. Discussion started: 11 December 2023

Recognizing that four decades may not provide a comprehensive understanding of decadal to multi-decadal variability, we expanded our analysis to more than a century, spanning from 1871 to 2020. As depicted in Figure S1, our century-long time series analysis reveals a noticeable multi-decadal variability in the 18-year moving correlation, which further validates our findings.

3.2. Potential forcing mechanisms underlying the variability in the SASD-ENSO relationship in the past four decades

We next explore what might be behind the decadal variability of the SASD-ENSO relationship (Figure 1). Since Niño 3 and Niño 4 have yielded results similar to those of Niño 3.4, the analyses here utilize Niño 3.4 only. We compare regressions of anomalous SST and atmospheric fields onto the Niño 3.4 index for the 2000-2020 period with those for the 1979-1999 period (Figures 2-4). For SST, the regression pattern appears to resemble more strongly the negative phase of the SASD index during 2000-2020 than during 1979-1999 (Figure 2a, b), seen as larger and more significant SST anomalies in the positive center of SASD during 2000-2020. Subtracting the 1979-1999 pattern from the 2000-2020 pattern yields a La Niña structure, where the values are negative in the eastern tropical Pacific but positive in the central and western tropical Pacific (Figure 2c), suggesting a shift to more central Pacific El Niño during the 2000-2020 period from more eastern Pacific El Niño during the 1979-1999 period.

Significant differences in the SST regression patterns indicating changes in ENSO

https://doi.org/10.5194/egusphere-2023-2436
Preprint. Discussion started: 11 December 2023

regime between the two periods are accompanied by substantial differences in the regression patterns of the top-of-the-atmosphere outgoing longwave radiation (OLR) and atmospheric circulations (see Figure 3). During the 1979-1999 period, there are negative OLR anomalies over the tropical Pacific Ocean and southeastern Pacific Ocean and positive anomalies over the southwestern Pacific Ocean and northern South America (Figure 3a). The negative OLR anomalies, an indication of more and stronger convective activities, produce positive Rossby Wave Source or RWS (Sardeshmukh and Hoskins, 1998) and upper-tropospheric divergent wind over the tropical and the southeastern Pacific Ocean and the opposite OLR anomalies generate negative RWS and upper-tropospheric convergent wind over the southwestern Pacific Ocean (Figure 3d). The sign of RWS determines the sign of vorticity and the direction of rotation in atmospheric waves, including Rossby waves. Specifically, positive (negative) RWS corresponds to positive (negative) relative vorticity or counterclockwise (clockwise) rotation of the upper atmosphere relative to the Earth's surface in the southern hemisphere. According to Sardeshmukh and Hoskins (1998), the components of RWS that represent the changes in vorticity include the advection of vorticity and vorticity anomalies related to the divergence of the flow. These vorticity anomalies propagate through teleconnection wavetrains. The negative RWS anomalies over the southwestern Pacific Ocean trigger a wavetrain that propagates southeastwards into the Ross Sea, then eastwards into the Amundsen, Bellingshausen, and Weddell Seas, as depicted by the anomalous fields of WAF and 200-hPa geopotential heights in Figure 4a. The wavetrain generates positive anomalies of the

https://doi.org/10.5194/egusphere-2023-2436
Preprint. Discussion started: 11 December 2023

mean sea level pressure (MSLP) over the South Atlantic north of 40°S and negative anomalies over the southeastern South Atlantic (Figure 4b).

The negative anomalous MSLP and cyclonic circulation result in a negative wind curl, which generates Ekman upwelling, leading to negative SST anomalies; the opposite occurs for positive MSLP and anticyclonic circulation (Chaves and Nobre, 2004). The negative SST anomalies along Brazil coasts are also related to coastal upwelling due to anomalous northeasterly winds (Franchito et al., 2008). Anomalous warm (cold) air advection induced by anomalous northerly (southwesterly) winds over the western South Atlantic Ocean also favors the formation of warm (cold) SST centers of the negative phase SASD through downward (upward) transfer of sensible heat flux (Figure 4b and 4d). Latent heat flux also plays an important role in the SST anomalies (Barreiro et al., 2004). The enhanced westerly wind anomalies also lower SST, which favors the development of the negative SST anomaly centers of the negative phase SASD. Downward longwave radiation also shows a dipole structure, which contributes to SST anomalies of the negative phase SASD (Figure S2a).

Compared to 1979-1999, the 2000-2020 period shows westward expansion of the positive OLR anomalies into the tropical western Pacific (Figure 3b). There is an increase in the extent, but a decrease in the magnitude, of the positive OLR anomalies over the southwestern Pacific Ocean, and an increase in the significance of the negative OLR anomalies over the central South Pacific Ocean. The OLR difference between the two periods shows a La Niña state (Figure 3c). Negative OLR anomalies indicating stronger than normal convective activities produce negative RWS and

https://doi.org/10.5194/egusphere-2023-2436
Preprint. Discussion started: 11 December 2023

upper-tropospheric convergence over the region east of New Zealand (Figure 3e), which excites a wavetrain propagating eastwards into South Atlantic Ocean (Figure 4c). Under the influence of this wavetrain, the anomalous MSLP field displays a dipole structure over the South Atlantic Ocean (Figure 4d). Similar to the discussion about the earlier period, the horizontal heat advection associated with the anomalous wind field, vertical heat transfer related to anomalous wind curl, and increased westerly winds all play an important role in the formation of the negative phase SASD. Weaker northeasterly wind anomalies relative to the earlier period weaken upwelling, leading to warmer SST anomalies. The stronger easterly wind anomalies over the eastern South Atlantic (25°S-30°S) offset the climatological southeasterly winds, contributing to the warm SST anomalies. Downward longwave radiation anomalies make larger contributions to the SST anomalies of the negative SASD than those over the former period (Figure S2).

The distinct regression patterns of the OLR, RWS, and upper-level divergent winds onto the Niño 3.4 index over the two periods (Figure 3c, f) suggest that the varying strengths of convective activities over the central South Pacific Ocean may have played an important role in the differences observed in the SASD-Niño 3.4 correlations between the two periods by triggering wavetrains propagating along different paths. Over the key region (20-40°S, 140-180°W) in the central South Pacific (green rectangle in Figure 3c), the correlation coefficients between the SASD index and the OLR anomalies are -0.16 ($p > 0.05$) for the 1979-1999 period and -0.66 ($p < 0.01$) for the 2000-2020 period. A comparison of the climatological SST and

https://doi.org/10.5194/egusphere-2023-2436
Preprint. Discussion started: 11 December 2023

OLR in this key region between the two periods shows a significant increase in SST and a decrease in OLR from the earlier to the latter period (Figure S3).

Besides the sources of the Rossby wavetrain, upper-level zonal wind also influences the propagating direction of the wavetrains by generating a Rossby waveguide. Climatological 200-hPa zonal wind display westerly winds south of 20 °S with the largest wind speed around 50° S (Figure 5a, b). Relative to the 1979-1999 period, stronger westerly winds at southern mid-latitudes during the 2000-2020 period help the wavetrain go into the waveguide and let it propagate eastwards and northeastwards into Southern Atlantic Ocean (Figure 4c). Conversely, during the 1979-1999 period, weaker westerly winds do not facilitate the wavetrain excited west of New Zealand go into the waveguide and the wavetrain only propagate southeastwards into the Ross and Amundsen Seas (Figure 4a).

In the past century, eastern Pacific ENSO events outnumbered the central Pacific ENSO events until near the end of the century, when the trend was reversed with the central Pacific events becoming more frequent (Kug et al., 2009; Freund et al., 2019). This shift in ENSO regime is reflected in Figure 2. According to Rodrigues et al. (2015), the two types of ENSO events trigger different atmospheric variability modes in the Southern Hemisphere represented by the Pacific South American (PSA) pattern. The central Pacific events trigger the third leading mode (PSA2; the first and second leading modes being AAO and PSA1, respectively) which, by modulating the strengths and position of the SASH, connects the tropical Pacific to the Atlantic. The teleconnection is absent during eastern Pacific ENSO events because these events

https://doi.org/10.5194/egusphere-2023-2436
Preprint. Discussion started: 11 December 2023

trigger PSA1. This helps explain the differences in the SASD-ENSO relationship between the two periods. The regressions of the SASD index onto the SST anomalies show that the spatial patterns of the Pacific SST anomalies corresponding to the positive phase SASD bear a resemblance to the eastern Pacific La Niña state over the former period, and to a central Pacific La Niña state over the latter period (Figure 6). The difference of the two patterns (2000-2020 minus 1979-1999) resembles a typical central Pacific La Niña state. It is, therefore, plausible that the stronger ENSO-SASD relationship during the recent two decades compared to the proceeding two decades could be related to the shift in the ENSO regime around the turn of the century from more frequent eastern Pacific El Niño to more frequent central Pacific El Niño.

To confirm the relationship between the OLR anomalies in the key region and the SASD anomalies, we conducted an idealized numerical experiment using the CAM5 atmospheric model. In this experiment, we artificially increase the SST by 2 ℃ in the key region (20 °S-40 °S, 180 °-140 °W), which corresponds to negative OLR anomalies (as depicted in Figure 2c and 3c). Figure 4S illustrates the anomalous 200-hPa geopotential height relative to the results from the control experiment, where SST and sea ice conditions followed the climatological annual cycle. Notably, a wavetrain is observed from the southern Pacific Ocean to the southern Atlantic Ocean. Additionally, the experiment shows a weakened South Atlantic Subtropical High (SASH) over the southern subtropical Atlantic Ocean. The corresponding 1000-hPa height and wind field display an anomalous low pressure and cyclonic circulation (Figure 5S), indicating a negative phase of the SASD. Although the OLR anomalies

https://doi.org/10.5194/egusphere-2023-2436
Preprint. Discussion started: 11 December 2023

are not entirely equivalent to SST anomalies, these numerical modeling results provide further evidence of the negative correlation between the OLR anomalies in the key region and the SASD.

It is important to note that the differences in the SST anomalies in the equatorial Pacific (as depicted in Figure 2c), which are indicative of varying ENSO conditions (i.e., a shifting from eastern to central Pacific El Nino regime around the turn of the century), laid the background for the OLR anomalies in the key region. Therefore, these differences played a critical role in modulating the SASD-ENSO teleconnection.

Two additional numerical experiments were conducted, where a +2 °C SST anomaly is introduced in the Niño 4 region over the central tropical Pacific (5 °N-5 °S, 160 °E-150 °W) and the Niño 3 region over the eastern tropical Pacific (5 °N-5 °S, 150 °W-90 °W), respectively, to ascertain the distinct impacts of eastern and central Pacific El Niño events on the ENSO-SASD relationship.

As depicted in Figures S6 and S7, in contrast to the idealized experiment involving SST anomalies over the eastern Pacific Ocean, the idealized experiment with the SST anomalies over the central Pacific Ocean resulted in geopotential height anomalies over the southern Atlantic Ocean shifting westward. This westward shift induced a surface cyclonic circulation, which favored the development of the negative phase of the SASD mode.

These numerical modeling results provide further confirmation that central Pacific El Niño events occurring more frequently after 2000 have a more pronounced impact on the ENSO-SASD relationship.

https://doi.org/10.5194/egusphere-2023-2436
Preprint. Discussion started: 11 December 2023

4. Conclusion and discussion

We have revisited the teleconnection of the SST variability in the subtropical Atlantic Ocean and tropical Pacific Ocean, represented by the SASD and Niño 3.4 indices, respectively. We have showed that SASD and Niño 3.4 are significantly correlated ($r = -0.51$, $p < 0.01$) over the past four decades, with a multi-decadal variability, which contradicts the weak simultaneous correlations between the two indices previously suggested in the literature (Venegas et al., 1997; Fauchereau et al., 2003; Hermes and Reason, 2005; Kayano et al., 2013; Rodrigues et al., 2015). We have also demonstrated a strengthening of their correlations over the recent two decades ($r = -0.77$, $p < 0.01$) from the preceding two decades ($r = -0.32$, $p > 0.05$), and this significant change in the correlation strength holds true when using either the Niño 4 index or Niño 3 index in place of the Niño 3.4 index. However, we acknowledge that the higher frequency of central El Nino events in recent years may have contributed to the stronger correlations. We have further confirmed the existence of the multi-decadal variability of the ENSO-SASD relationship through analysis of century-long SST time series.

Furthermore, we have demonstrated that the changes in the relationship between SASD and ENSO from the earlier two decades to the recent two decades are not only associated with the shift in ENSO regime but may also be directly linked to differences in the anomalous SST and convective activity reflected in OLR anomalies in the crucial region (20°S-40°S, 180°-140°W) of the central South Pacific Ocean. These variations, together with differences in upper-level zonal winds, cause

https://doi.org/10.5194/egusphere-2023-2436
Preprint. Discussion started: 11 December 2023

wavetrains triggered by varying convective activities to propagate along distinct paths, inducing varying responses in the anomalous MSLP, surface wind, and downward longwave radiation fields, ultimately resulting in differences in SST anomalies in the subtropical Atlantic Ocean.

The significant strengthening of the SASD-ENSO relationship in recent decades may also be related to the sudden phase reversal of the interdecadal-scale modes in the Pacific and the Atlantic Oceans near the end of the last century (Yu et al., 2017). In particularly, the Pacific Decadal Oscillation (PDO) and the Interdecadal Pacific Oscillation (IPO) shifted from positive to negative phase while the opposite occurred to the Atlantic Multidecadal Oscillation (AMO) around 2000. Salinger et al. (2001) noted that IPO has a strong influence on the relationship between the ENSO index and South Pacific precipitation. The positive phase of IPO favors the negative phase of SASD on interdecadal time scales (Lopez et al., 2016). How IPO (PDO) may influence the SASD-ENSO relationship remains to be explored in future studies. Additionally, the tropical passage between the tropical Pacific and Atlantic Oceans may also influence their relationship (Giannini et al., 2001; Seager et al., 2019). Ham et al. (2021) found that the SASD mode influences ENSO through tropical Atlantic SST anomalies and the zonal Walker circulation. Our results further highlight aspects of the complexity of the interactions between the South Atlantic and Pacific SST variations. Further exploration of the influence of the IPO and PDO on the SASD-ENSO relationship, as well as the tropical passage between the Pacific and Atlantic Oceans, is needed to gain a deeper understanding of the complex interactions between these coupled atmosphere-ocean systems.

Our study focuses on the simultaneous SASD-ENSO relationship, the SST dipole structure of the SASD during austral summer (JFM) also may be associated with the ENSO forcing in previous spring (OND) and winter (JJA) due to the delayed response of the ocean mixed layer (Saravanan and Chang, 2000; Fernandez and Barreiro, 2022).

In addition to natural variability discussed here, global climate change also may influence the SASD-ENSO relationship, because global warming may change the characteristics of ENSO and atmospheric teleconnections related to ENSO (Martín-Gómez et al., 2020a; Martín-Gómez et al., 2020b; Martín-Gómez and Barreiro, 2020; Cai et al., 2021;).

Our study contributes to the growing body of knowledge on the interactions between the South Atlantic and Pacific SST variations, which have a strong influence on South American and southern African rainfall patterns (Kayano et al., 2013). The knowledge gained from our study may also improve possibilities for sub-seasonal to seasonal predictions of precipitation in these regions.

Code and data availability

The monthly SST data from the U.S. NOAA Extended Reconstructed Sea Surface Temperature (ERSST) version 5 (ERSST v5) are available online (https://www1.ncdc.noaa.gov/pub/data/cmb/ersst/v5/netcdf/). The ERA5 reanalysis data are available from the below website (https://doi.org/10.24381/cds.6860a573). The monthly OLR data are derived from the website (https://psl.noaa.gov/data/gridded/data.uninterp_OLR.html). The monthly SST and OLR data from 20 models of CMIP6 for SSP1-2.6, SSP2-4.5, and SSP 3-7.0 scenarios are derived from the website (https://aims2.llnl.gov/search).

Code is available upon request to corresponding author.

Acknowledgements

We thank the European Centre for Medium-Range Weather Forecasts (ECMWF) for the ERA5 data. This study is financially supported by, the National Key R&D Program of China (2022YFE0106300), and the European Commission H2020 project Polar Regions in the Earth System (PolarRES; Grant101003590).

Author contributions

The research was designed by Lejiang Yu, who also analyzed the data and wrote the initial draft. Shiyuan Zhong contributed significantly to the writing during both the initial submission and revision stages. Timo Vihma provided valuable consultation to the research, while Cuijuan Sui helped with the analysis of sea ice data. Bo Sun provided comments and played a key role in securing funding for the research. All authors have reviewed and contributed to the final manuscript

Competing interests

The authors declare no competing interests.

References

Barreiro M, Giannini A, Chang P and Saravanan R 2004 On the role of the South Atlantic atmospheric circulation in tropical Atlantic variability Geophysical Monograph Series, editor Wang, C. Xie, S.P., Carton, J. A.

Bombardi R J and Carvalho L M V 2011 The South Atlantic dipole and variations in the characteristics of the South American monsoon in the WCRP-CMIP3 multi-model simulations *Clim. Dyn.* **36** 2091-2102

Bombardi R J, Carvalho L M V, Jones C and Reboita M S 2014 Precipitation over eastern South America and the South Atlantic sea surface temperature during neutral ENSO periods *Clim. Dyn.* **42** 1553-1568

Cai W et al. 2021 Changing El Nino-Southern oscillation in a warming climate *Nature Reviews Earth & Environment* **2** 628-644.

Chaves R R and Nobre P 2004 Interactions between sea surface temperature over the South Atlantic Ocean and the South Atlantic convergence zone *Geophys. Res. Lett.* **31** L03204

Clogg C C, Petkova E and Haritou A (1995). Statistical methods for comparing regression coefficients between models *Am. J. Sociol.* **100**, 1261-1293.

Colberg F and Reason C J C 2006 Ocean model diagnosis of low-frequency climate variability in the South Atlantic region *J. Climate* **20** 1016-1034

Fauchereau N, Trzaska S, Richard Y, Roucou P and Camberlin P 2003 Sea surface temperature co-variability in the Southern Atlantic and Indian Oceans and its connections with the atmospheric circulation in the Southern Hemisphere. *Int. J. Climatol.* **23** 663–677

Fernandez P and Barreiro M 2022 A late ‘80s shift in El Niño influence on rainfall over Uruguay during austral spring *Int. J. Climatol.* ***42*** 6844-6858

Franchito S H, Oda T O, Rao V B and Kayano M 2008 Interation between coastal upwelling and local winds at Cabo Frio, Bazil: An observational study *J. Appl. Meteorol. Climatol.* **47** 1590-1598

Freund M B, Henley B J, Karoly D J, McGregor H V, Abram N J and Dommenget D 2019 Higher frequency of Central Pacific El Nino events in recent decades relative to past centuries *Nat. Geosci.* 12 450-455

Giannini A, Chiang C H, Cane M A, Kushnir Y and Seager R 2001 The ENSO teleconnection to the tropical Atlantic Ocean: Contributions of the remote and local SSTs to rainfall variability in the tropical Americas *J. Climate* **14** 4530-4544

Haarsma . J, Campos E J D, Hazeleger W, Severijns C, Piola A R and Molteni F 2005 Dominate modes of variability in the South Atlantic: A study with a hierarchy of ocean=atmosphere models *J. Climate* **18** 1719-1735

Ham Y-G, Lee H-J, Jo H-S, Lee S-G, Cai W and Rodrigues R R 2021 Inter-basin

https://doi.org/10.5194/egusphere-2023-2436
Preprint. Discussion started: 11 December 2023

interaction between variability in the South Atlantic Ocean and the El Ni ño/Southern Oscillation *Geophys. Res. Lett.* **48** e2021GL093338

Hermes J C and Reason C J C 2005 Ocean model diagnosis of interannual coevolving SST variability in the South Indian and South Atlantic oceans *J. Climate* **18** 2864-2882

Hersbach H et al. 2020 the ERA5 global reanalysis *Q. J. Roy. Meteor. Soc.* **146** 1999-2049

Huang B, Thorne P W, Banzon V F and Zhang H M 2017 Extended reconstructed Sea surface Temperature version 5 (ERSSTv5), Upgrades, validations, and Intercomparisons *J. Climate* **30** 8179-8205

Kayano M T, Andreoli R V and Ferreira de Souza R A 2013 Relations between ENSO and the South Atlantic SST modes and their effects on the South American rainfall *Int. J. Climatol.* **33** 2008–2023

Kao H Y and Yu J Y (2009). Contrasting eastern-Pacific and central-Pacific types of ENSO *J. Climate* **22**, 615-632

Kug J-S, Jin F-F and An S-J 2009 Two types of El Niño events: cold tongue El Niño and Warm pool El Niño *J. Climate* **22** 1499-1515

Liebmann B and Smith C A 1996 Description of a complete (interpolated outgoing longwave radiation dataset *Bull. Amer. Meteor. Soc.* **77** 1275-1277

Lin Z 2019 the South Atlantic-South Indian Ocean pattern: a zonally oriented teleconnection along the Southern Hemisphere westerly jet in austral summer *Atmosphere* **10** 259

Lopez H, Dong S, Lee S-K and Campos E 2016 Remote influence of interdecada l Pacific Oscillation on the South Atlantic meridional overturning circulation variability *Geophys. Res. Lett.* **43** 8250-8258

Mart ín-G ómez V, Barreiro M, Losada T and Rodr íguez-Fonseca B 2020a Southern hemisphere circulation anomalies and impacts over subtropical South America due to different El Ni ño flavours *Int. J. Climatol.* **40** 6201-6218

Mart ín-G ómez V, Barreiro M and Mohino E 2020b Southern Hemisphere sensitivity to ENSO Patterns and Intensities: Impacts over Subtropical South America

https://doi.org/10.5194/egusphere-2023-2436
Preprint. Discussion started: 11 December 2023

Atmosphere **11** 77

Martín-Gómez V and Barreiro M 2020 The influence of nonlinearities and different SST spatial patterns on the summertime anomalies in subtropical South America during strong ENSO events *Clim. Dyn.* **54** 3765-3779

Morioka Y, Tozuka T, Masson S, Terray P, Luo J-J and Yamagata T 2012 Subtropical dipole modes simulated in a coupled general Circulation mode *J. Climate* **25** 4029-4047

Morioka Y, Tozuka T and Yamagata T 2011 On the growth and decay of the subtropical dipole mode in the South Atlantic *J. Climate* **24** 5538-5554

Morioka Y, Masson S, Terray P, Prodhomme C, Behera S K and Masumoto Y 2014 Role of tropical SST variability on the formation of subtropical dipoles *J. Climate 27* 4486-4507

Muza M N, Carvalho L M V, Jones C and Liebmann B 2009 Intraseasonal and interannual variability of extreme dry and wet events over southeastern South America and the subtropical Atlantic during austral summer *J. Climate* **22** 1682–1699

Nnamchi H C and Li J 2011 Influence of the South Atlantic Ocean dipole on West African summer precipitation *J. Climate* **24** 1184–1197

1. Neale R B, Richter J H, Conley A J, et al. 2011. Description of the NCAR community atmosphere Model(CAM5). Technical Report NCAR/TN-486+STR. Boulder, Colorado: National Center for Atmospheric Research, 268.

Rodrigues R R, Campos E J D and Haarsma R 2015 The impact of ENSO on the South Atlantic subtropical dipole mode *J. Climate* **28** 2691-2705.

Salinger M J. Renwick J A and Mullan A B 2001 Interdecadal Pacific oscillation and South Pacific climate *Int. J. Climatol.* **21** 1705-1721

Sardeshmukh P D and Hoskins B J 1988 The generation of global rotational flow by steady idealized tropical divergence *J. Atmos. Sci*. **45** 1228-1251

Saravanan R and Chang P 2000 Interaction between tropical Atlantic variability and El Nino-Southern Oscillation *J. Climate* **13** 2177-2194

Seager R, Cane M, Henderson N, Lee D-E, Abernathey R and Zhang H 2019

https://doi.org/10.5194/egusphere-2023-2436
Preprint. Discussion started: 11 December 2023

Strengthening tropical Pacific zonal sea surface temperature gradient consistent with rising greenhouse gases *Nat. Clim. Change* **9** 517-522

Sterl A and Hazeleger W 2003 Coupled variability and air-sea interaction in the South Atlantic Ocean *Clim. Dyn.* 21 559-571

Takaya K and Nakamura H 2001 A formulation of a phase in dependent wave-activity flux for stationary and migratory quasi geostrophic eddies on a zonally varying basic flow *J. Atmos. Sci.* **58** 608-627

Trenberth K E 1997 The Definition of El Niño *Bull. Amer. Meteor. Soc.* **78** 2771–2777

Venegas S A, Mysak L A and Straub D N 1997 Atmosphere-ocean coupled variability in the South Atlantic *J. Climate* **10** 2904-2920

Vigaud N, Richard Y, Rouault V and Fauchereau N 2009 Moisture transport between the South Atlantic Ocean and southern Africa: Relationships with summer rainfall and associated dynamic *Clim. Dyn.* **32** 113-123

Yu L, et al. (2017). Possible connection of the opposite trends in Arctic and Antarctic sea ice cover *Sci. Rep.* **7** 45804

Yu L, Zhong S, Vihma T, Sui C and Sun B (2023). A change in the relation between The Subtropical Indian Ocean Dipole and the South Atlantic Ocean Dipole indices in the past four decades *Atmospheric Chem. Phys*. **23** 345-353

https://doi.org/10.5194/egusphere-2023-2436
Preprint. Discussion started: 11 December 2023

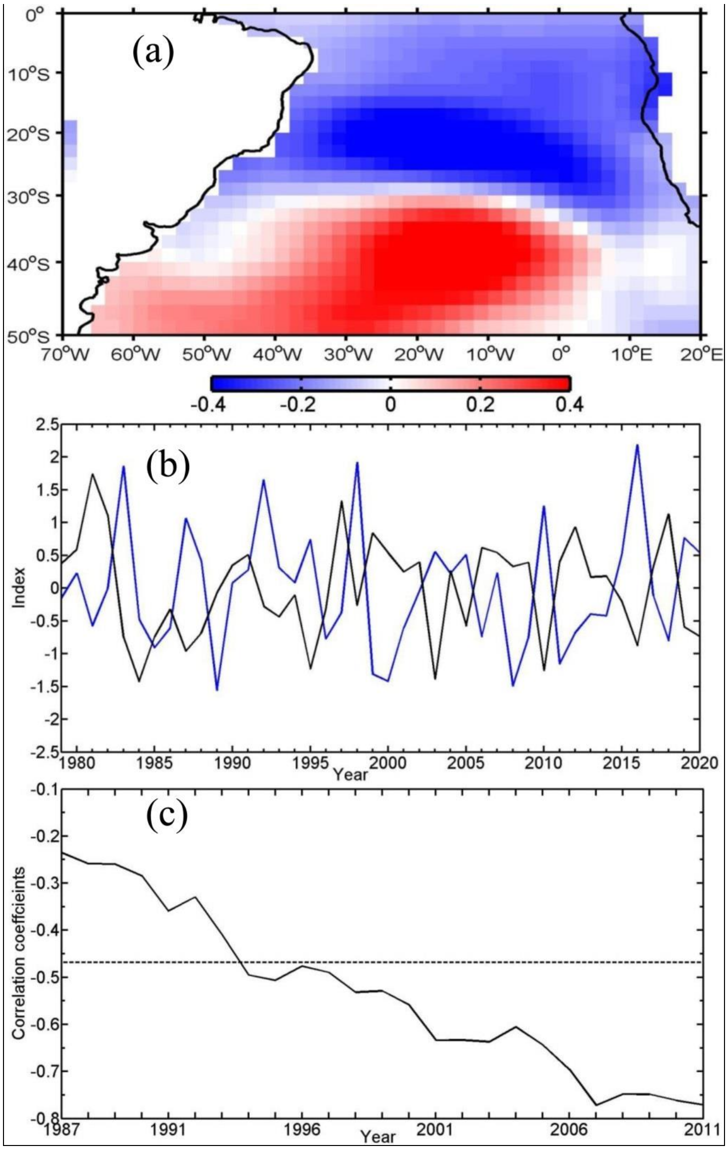

Figure 1. The spatial pattern of SST for the positive SASD phase (a), the time coefficients of the detrended Niño 3.4 (solid blue lines) and SASD (solid black lines) indices in austral summer (JFM) (b), and the 18-year moving correlations between the two indices (black sold line) (c).The dashed line in (c) denotes the correlation coefficients with the above 95% confidence. The number of abscissa denotes the middle of 18-year sliding window. For example, 1987 is the middle year of 1979-1996 period.

https://doi.org/10.5194/egusphere-2023-2436
Preprint. Discussion started: 11 December 2023

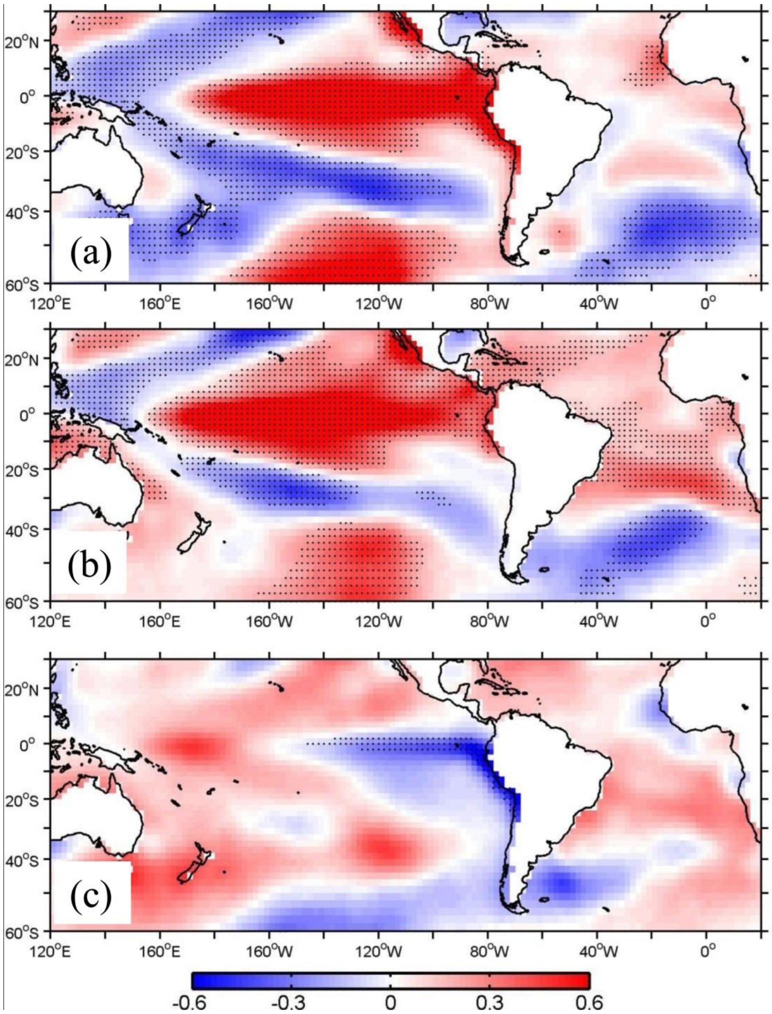

Figure 2. Regression maps of SST anomalies (°C) onto the Niño 3.4 index over the 1979-1999 period (a) and the 2000-2020 period (b) and the difference between them (b-a) (c). Dotted regions denote the above 95% confidence level.

https://doi.org/10.5194/egusphere-2023-2436
Preprint. Discussion started: 11 December 2023

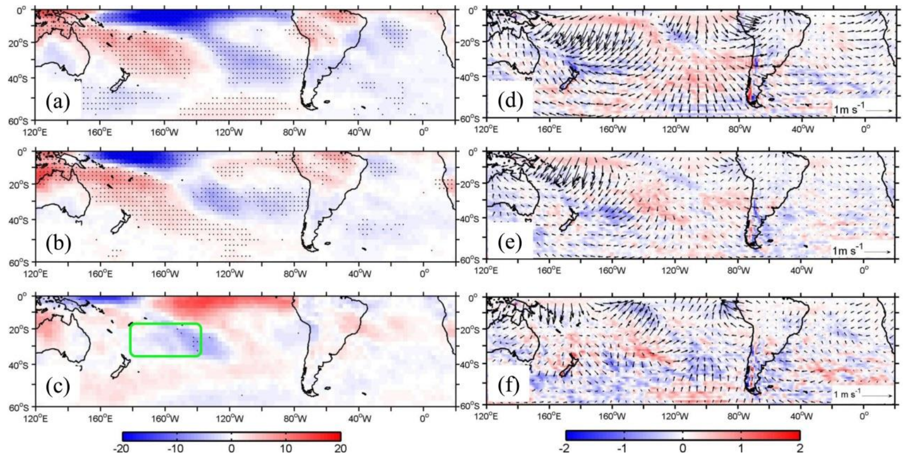

Figure 3. Regression maps of anomalous fields of OLR (W m^{-2}) (a), (b), (c), Rossby wave source (RWS) ($10^{-10}\,s^{-2}$) and 200-hPa divergent wind (vector) (d), (e), (f) onto the Nino 3.4 index over the periods of 1979-1999 (a, d), 2000-2020 (b, e) and the differences between the two periods (latter minus former) (c, f). Dotted regions in panels (a), (b) and (c) denote the above 95% confidence level. The green box in panel c indicates the key region of OLR.

https://doi.org/10.5194/egusphere-2023-2436
Preprint. Discussion started: 11 December 2023

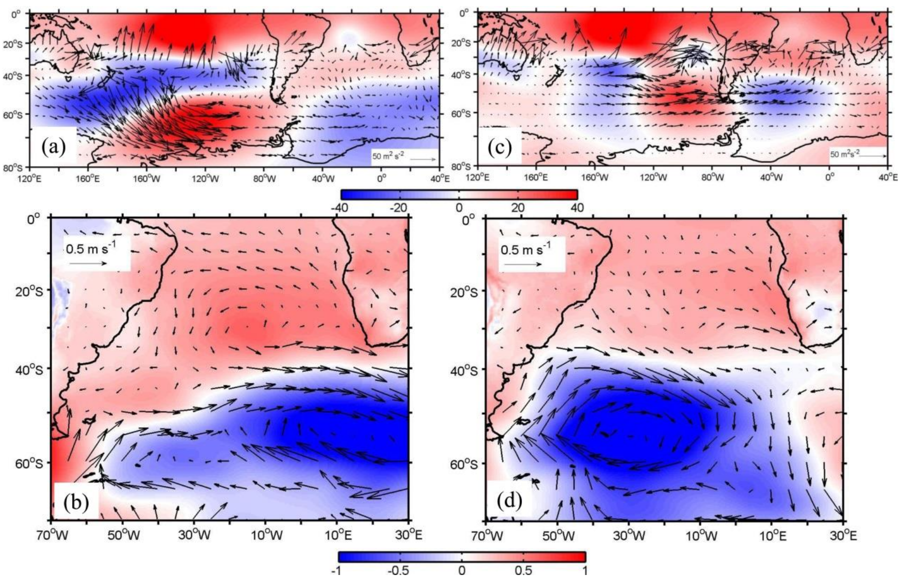

Figure 4. Regression maps of the anomalous fields of WAF (vector) and 200-hPa geopotential height (gpm) (a, c), and mean sea level pressure (hectopascal) and surface wind (vector) (b, d) onto the Nino 3.4 index over the periods of 1979-1999 (a, b) and 2000-2020 (c, d).

https://doi.org/10.5194/egusphere-2023-2436
Preprint. Discussion started: 11 December 2023

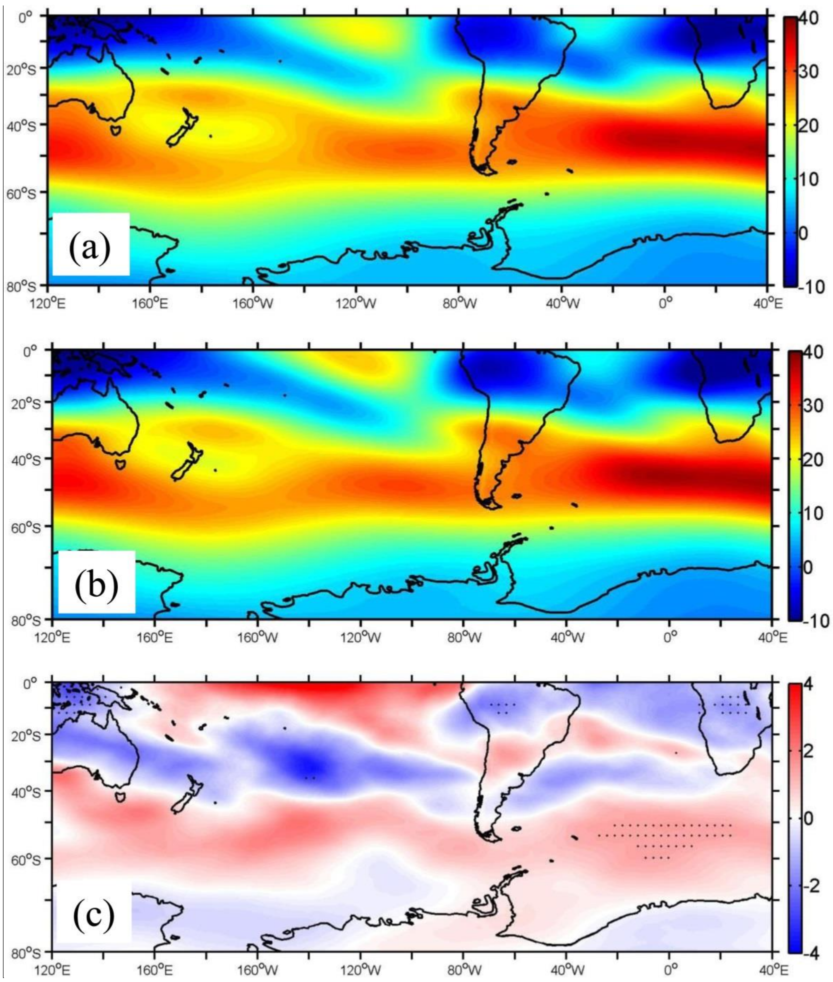

Figure 5. Climatological summertime 200-hPa zonal wind speed (m s^{-1}) for the 1979-1999 period (a), for the 2000-2020 period (b) and their difference (c). Dotted regions in panel c denote above 95% confidence level.

https://doi.org/10.5194/egusphere-2023-2436
Preprint. Discussion started: 11 December 2023

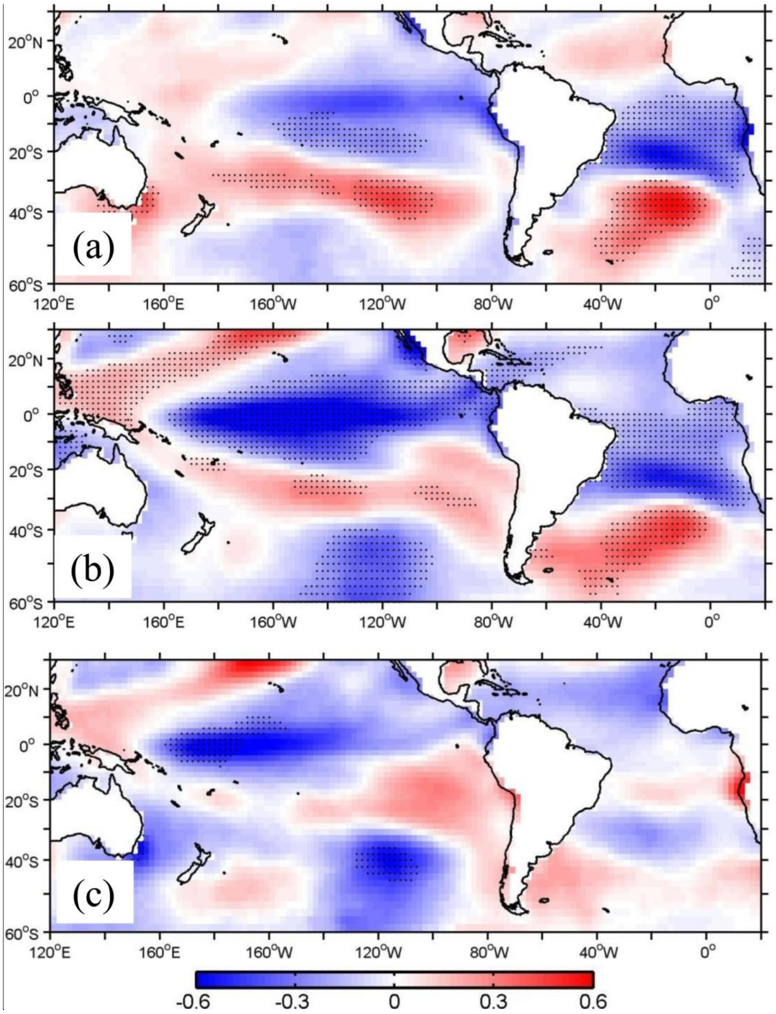

Figure 6. Regression maps of SST anomalies (°C) onto the SASD index for austral summer over the periods of 1979-1999 (a), 2000-2020 (b), and the differences between them (b-a) (c). Dotted regions denote the above 95% confidence level.